Bioelectric Navigation: A New Paradigm for Intravascular Device Guidance

Bernhard Fuerst[1,2(✉)], Erin E. Sutton[1,3], Reza Ghotbi[4], Noah J. Cowan[3], and Nassir Navab[1,2]

[1] Computer Aided Medical Procedures, Johns Hopkins University, Baltimore, MD, USA
{be.fuerst,esutton5}@jhu.edu
[2] Computer Aided Medical Procedures, Technische Universität München, Munich, Germany
[3] Department of Mechanical Engineering, Johns Hopkins University, Baltimore, MD, USA
[4] Department of Vascular Surgery, HELIOS Klinikum München West, Munich, Germany

Abstract. Inspired by the electrolocalization behavior of weakly electric fish, we introduce a novel catheter guidance system for interventional vascular procedures. Impedance measurements from electrodes on the catheter form an electric image of the internal geometry of the vessel. That electric image is then mapped to a pre-interventional model to determine the relative position of the catheter within the vessel tree. The catheter's measurement of its surroundings is unaffected by movement of the surrounding tissue, so there is no need for deformable 2D/3D image registration. Experiments in a synthetic vessel tree and *ex vivo* biological tissue are presented. We employed dynamic time warping to map the empirical data to the pre-interventional simulation, and our system correctly identified the catheter's path in 25/30 trials in a synthetic phantom and 9/9 trials in biological tissue. These first results demonstrated the capability and potential of Bioelectric Navigation as a non-ionizing technique to guide intravascular devices.

1 Introduction

As common vascular procedures become less invasive, the need for advanced catheter navigation techniques grows. These procedures depend on accurate navigation of endovascular devices, but the clinical state of the art presents significant challenges. In practice, the interventionalist plans the path to the area of interest based on pre-interventional images, inserts guide wires and catheters, and navigates to the area of interest using multiple fluoroscopic images. However, it is difficult and time-consuming to identify bifurcations for navigation, and the challenge is compounded by anatomic irregularities.

B. Fuerst and E.E. Sutton are joint first authors, having contributed equally.

S. Ourselin et al. (Eds.): MICCAI 2016, Part I, LNCS 9900, pp. 474–481, 2016.
DOI: 10.1007/978-3-319-46720-7_55

Previous work has focused interventional and pre-interventional image registration [2,3,9], but adopting those techniques to endovascular navigation requires deformable registration, a task that has proven challenging due to significant vessel deformation [1]. From a clinical standpoint, the interventionalist is interested in the catheter's position within the vessel tree, and deformation is irrelevant to navigation since the catheter is constrained to stay within the tree. In fact, to guide the catheter, one only needs a series of consecutive local measurements of its surroundings to identify the branch and excursion into the branch. This suggests that a sensor directly on the catheter could be employed for navigation.

In this paper, we propose a radical new solution, Bioelectric Navigation. It was inspired by the weakly electric fish which generates an electric field to detect subtle features of nearby objects [4]. Our technique combines such local impedance measurements with estimates from pre-interventional imaging to determine the position of catheter within the vascular tree (Fig. 1). Instead of the interventionalist relying on fluoroscopy, the catheter itself is equipped with electrodes to provide feedback. One or more of the electrodes on the catheter emits a weak electric signal and measures the change to the resulting electric field as the catheter advances through the vessel tree. The impedance of blood is much lower than that of vessel walls and surrounding tissue [5], so the catheter detects local vessel geometry from measured impedance changes. For instance, as the device passes a bifurcation, it detects a significant disturbance to the electric field caused by the dramatic increase in vessel cross-sectional area. Bioimpedance analysis has been proposed for plaque classification [8] and vessel lumen measurement [7,12] but, to our knowledge, has not been applied to navigation. The relative ordering and amplitude of the features (e.g. bifurcations, stenoses) used for matching the live signal to the pre-interventional estimate are unchanged under deformation, so the system is unaffected by movement and manipulation of the surrounding tissue and does not require 2D/3D deformable registration.

Fig. 1. In Bioelectric Navigation, live bioelectric measurements are registered to simulated signals from a pre-interventional image to identify the catheter's position.

In our novel system, the local measurement from the catheter is compared to predicted measurements from a pre-interventional image to identify the global position of the catheter relative to the vessel tree. It takes advantage of high-resolution pre-interventional images and live voltage measurement for improved device navigation. Its primary benefit would be the reduction of radiation exposure for the patient, interventionalist, and staff. Experiments in a synthetic vessel tree and *ex vivo* biological tissue show the potential of the proposed technology.

2 Materials and Methods

2.1 Modeling Bioimpedance as a Function of Catheter Location

The first step in Bioelectric Navigation is the creation of a bioimpedance model from the pre-interventional image. A complete bioimpedance model requires solution of the 3D Poisson equation, assuming known permittivities of blood and tissue. Given a relatively simple geometry, one can employ finite element analysis to numerically solve for the electric potential distribution. For our first feasibility experiments, we designed an eight-path vessel phantom with two stenoses and one aneurysm. We imported the 3D CAD model into Comsol Multiphysics (COMSOL, Inc., Stockholm, Sweden) and simulated the signal as a two-electrode catheter passed through the six primary branches (Fig. 2A). The simulation yielded six distinct models, one for each path.

2.2 Cross-Sectional Area to Parameterize Vessel Tree

It is unfeasible to import the geometry of an entire human cardiovascular system and simulate every path from a given insertion site. However, for catheter navigation, we are only interested in temporal variation of the measured signal as the catheter travels through the vascular tree. This is why sensing technologies such as intravascular ultrasound and optical coherence tomography are excessive for catheter navigation. Instead of an exact characterization of the vessel wall at each location, we use a simpler parameter to characterize the vessel geometry: cross-sectional area along the centerline of a vessel. We model the blood between the emitting electrode and the ground electrode as an RC circuit, so the voltage magnitude at the emitting electrode is inversely proportional to the cross-sectional area of the vessel between the two electrodes, greatly simplifying our parameterization of the vessel tree.

There are many methods for the segmentation of the vascular tree in CT images, and selecting the optimal method is not a contribution of this work. In fact, our system is largely invariant to the segmentation algorithm chosen. It uses the relative variation between segments to guide the catheter, so as long as it captures major geometric features, the extracted model need not have high resolution. Here, we selected segmentation parameters specific to the imaging modality (e.g. threshold, shape, background suppression) based on published techniques [6,10]. After manual initialization at an entry point, the algorithm detected the centerline and the shortest path between two points in a vessel-like segmentation. It generated the vessel model and computed the cross-sectional area at each segment for each possible path.

For the synthetic phantom, the simulated voltage at the emitting electrode was proportional to the inverse of the cross-sectional area extracted from the cone-beam CT (CBCT) (Fig. 2B). We conclude that cross-sectional area is adequate for localization with a two-electrode catheter, the minimum required for Bioelectric Navigation.

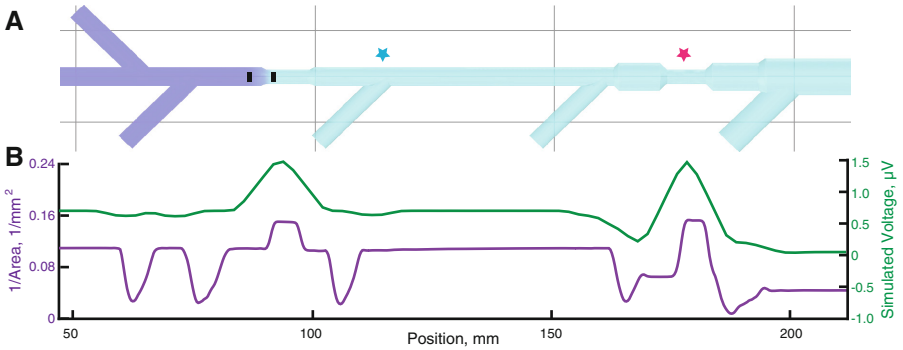

Fig. 2. (A) Simulation of synthetic vessel phantom from imported CAD geometry. The electrodes (black) span the left-most stenosis in this image. The voltage decreases at a bifurcation (blue star) and increases at a stenosis (pink star). **(B)** Simulated voltage magnitude (green) and the inverse of the cross-sectional area (purple) from the segmented CBCT.

2.3 Bioimpedance Acquisition

Like the fish, the catheter measures changes to its electric field to detect changes in the geometry of its surroundings. The bioimpedance acquisition consists of three main components: the catheter, the electronics, and the signal processing. Almost any commercially available catheter equipped with electrodes can be used to measure bioimpedance. A function generator supplies a sinusoidal input to a custom-designed constant current source. The current source supplies a constant low-current signal to the emitting electrode on the catheter, creating a weak electric field in its near surroundings. As such, the voltage measured by the catheter is a function of the change in impedance. Our software simply extracts the voltage magnitude at the input frequency as the catheter advances.

2.4 Modeled and Empirical Signal Matching

The bioimpedance signal is a scaled and time-warped version of the inverse cross-sectional area of the vessel, so the alignment of measured bioimpedance from the catheter with the modeled vessel tree is the foundation of our technique. While we are investigating other alignment methods, in these initial experiments we used open-ended dynamic time warping (OE-DTW) [11]. OE-DTW was chosen because it can be adapted to provide feedback to the interventionalist during a procedure. OE-DTW enables the alignment of incomplete test time series with complete references. The incomplete voltage series during a procedure is incrementally compared to each of the complete references from the model to obtain constant feedback about the predicted location of the catheter. See [11] for details. In our implementation, inverse cross-sectional area along each path formed the reference dataset, and the voltage magnitude from the catheter was the test time series. It estimated the most likely position of the catheter in

the vessel model by identifying the reference path with the highest similarity measure: the normalized cross-correlation with the test signal. In these initial experiments, we advanced the catheter through approximately 90 % of each path, so our analysis did not take advantage of the open-ended nature of the algorithm.

3 Experiments and Results

3.1 Experimental Setup

The prototype was kept constant for the two experiments presented here (Fig. 3). We used a 6 F cardiac electrophysiology catheter (MutliCath 10J, Biotronik, Berlin, Germany). Its ten ring electrodes were 2 mm wide with 5 mm spacing. The input to the current source was ±5 mV at 430 Hz, and the current source supplied a constant 18 μA to the emitting electrode. A neighboring electrode was grounded. The voltage between the two electrodes was amplified and filtered by a low-power biosignal acquisition system (RHD2000, Intan Technologies, Los Angeles, USA). The Intan software (Intan Interface 1.4.2, Intan Technologies, Los Angeles, USA) logged the signal from the electrodes. A windowed discrete Fourier transform converted the signal into the frequency domain, and the magnitude at the input frequency was extracted from each window. The most likely path was identified as described in Sect. 2.4. While real-time implementation is crucial to navigation, these first experiments involved only post hoc analyses.

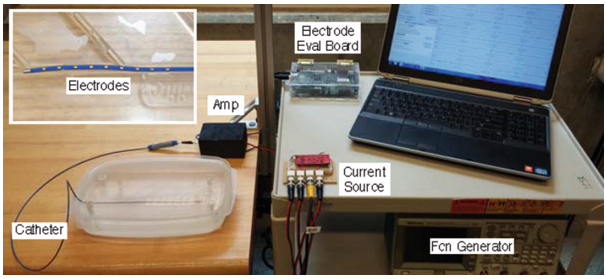

Fig. 3. A function generator supplied a sinusoidal signal to the current source, creating a weak electric field around the catheter tip. Electrodes on the catheter recorded the voltage as it was pulled through six paths of the phantom. Inset: catheter in phantom.

3.2 Synthetic Vessel Tree

We performed the first validation experiments in the synthetic vessel tree immersed in 0.9 % saline (Fig. 4). A camera recorded the trajectory of the catheter through the phantom as it advanced through the six main paths at 1–2 mm/s. The OE-DTW algorithm correctly identified the path taken in 25/30 trials. The similarity measure was 0.5245 ± 0.0683 for misidentified trials and 0.6751 ± 0.1051 for correctly identified trials.

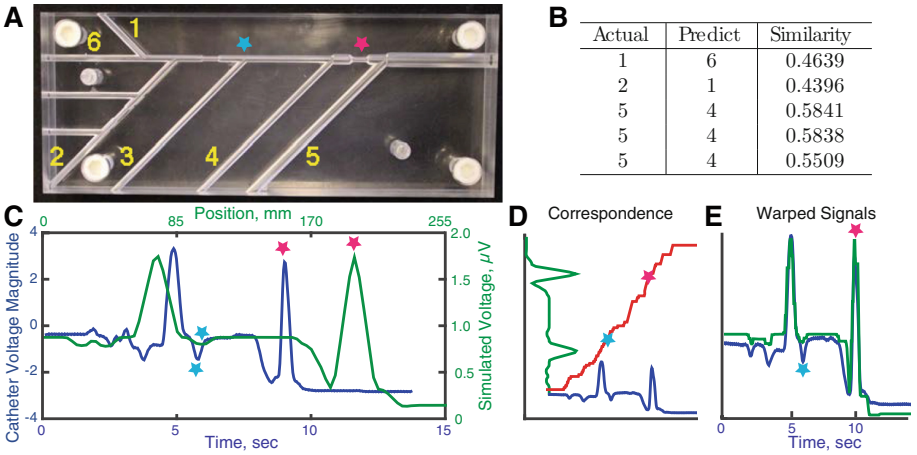

Actual	Predict	Similarity
1	6	0.4639
2	1	0.4396
5	4	0.5841
5	4	0.5838
5	4	0.5509

Fig. 4. **(A)** Synthetic phantom with labeled paths. The two halves of the phantom were machined from acrylic and sealed with a thin layer of transparent waterproof grease. When assembled, it measured 10 cm × 25.4 cm × 5 cm. **(B)** Trials for which OE-DTW incorrectly predicted catheter position. **(C)** The measured voltage (blue) and the simulated signal (green) identify the two stenoses and four bifurcations. The signals appear correlated but misaligned. **(D)** The OE-DTW algorithm found a correspondence path between the two signals. **(E)** OE-DTW aligned the simulated data to the measured data and calculated the cross-correlation between the two signals.

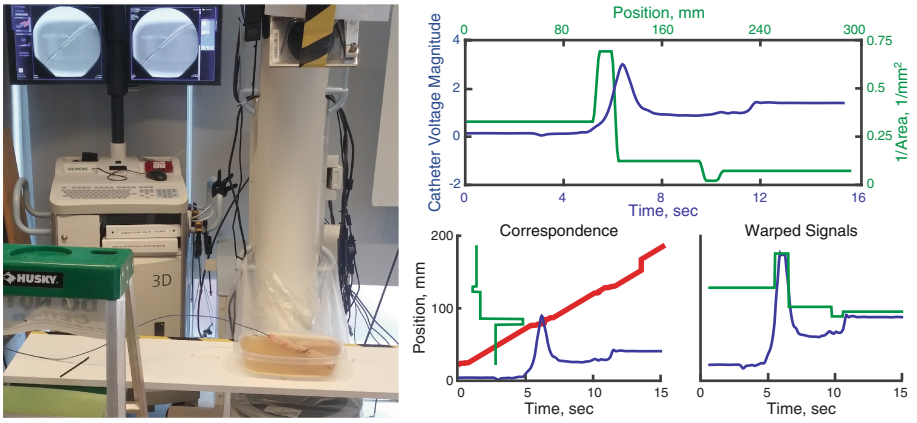

Fig. 5. Biological tissue experiment (left) and results from one trial in the long path (right). The stenosis and bifurcation are visible in both the inverse of the cross-sectional area and voltage magnitude.

3.3 *Ex Vivo* Aorta

The impedance difference between saline and vessel is less dramatic than between saline and acrylic, so we expected lower amplitude signals in biological tissue. We sutured two porcine aorta into a Y-shaped vessel tree and simulated a stenosis

in the trunk with a cable tie. We embedded the vessel in a 20 % gelatin solution and filled the vessel with 0.9 % saline. The ground truth catheter position was recorded from fluoroscopic image series collected simultaneously with the voltage measurements (Fig. 5). The catheter was advanced six times through the long path and three times through the short path. The algorithm correctly identified the path 9/9 times with similarity measure 0.6081 ± 0.1614.

4 Discussion

This preliminary investigation suggests that the location of the catheter in a blood vessel can be estimated by comparing a series of local measurements to simulated bioimpedance measurements from a pre-interventional image.

Our technology will benefit from further integration of sensing and imaging before clinical validation. While OE-DTW did not perfectly predict the location of the catheter, the trials for which the algorithm misclassified the path also had the lowest similarity scores. In practice, the system would prompt the interventionalist to take a fluoroscopic image when similarity is low. Because it measures local changes in bioimpedance, we expect the highest accuracy in feature-rich environments, those most relevant to endovascular procedures. The estimate is least accurate in low-feature environments like a long, uniform vessel, but as soon as the catheter reaches the next landmark, the real-time location prediction is limited only by the resolution of the electric image from the catheter. A possible source of uncertainty is the catheter's position in the vessel cross-section relative to the centerline, but according to our simulations and the literature [12], it does not significantly impact the voltage measurement.

To display the real-time position estimate, our next step is to compare techniques that match simulated and live data in real time (e.g. OE-DTW, Hidden Markov Models, random forests, and particle filters). A limitation of these matching algorithms is that they fail when the catheter changes direction (insertion vs retraction). One way we plan to address this is by attaching a simple encoder to the introducer sheath to detect the catheter's heading and prompting our software to only analyze data from when the catheter is being inserted. We recently validated Bioelectric Navigation in biologically relevant flow in the synthetic phantom and performed successful renal artery detection the the abdominal aorta of a sheep cadaver model. Currently, we are evaluating the prototype's performance *in vivo*, navigating through the abdominal vasculature of swine.

5 Scientific and Clinical Context

The generation and measurement of bioelectrical signals within vessels and their mapping to a patient-specific vessel model has never been proposed for catheter navigation. This work is complementary to the research done within MICCAI community and has the potential to advance image-guided intervention. Bioelectric Navigation circumvents many clinical imaging challenges such as catheter detection, motion compensation, and catheter tracking. Significantly, deformable

registration for global 3D localization becomes irrelevant; the interventionalist may move a vessel, but the catheter remains in the same vascular branch.

Once incorporated into the clinical workflow, Bioelectric Navigation has the potential to significantly reduce fluoroscope use during common endovascular procedures. In addition, it could ease the positioning of complex grafts, for instance a graft to repair abdominal aortic aneurysm. These custom grafts incorporate holes such that the the visceral arterial ostia are not occluded. Angiographic imaging is of limited use to the positioning of the device because the operator must study the graft markers and arterial anatomy simultaneously. In contrast, when the bioelectric catheter passes a bifurcation, the electric impedance changes dramatically. Bioelectric Navigation's inside-out sensing could change the current practice for device deployment by providing real-time feedback about device positioning from inside the device itself.

References

1. Ambrosini, P., Ruijters, D., Niessen, W.J., Moelker, A., van Walsum, T.: Continuous roadmapping in liver TACE procedures using 2D–3D catheter-based registration. Int. J. CARS **10**, 1357–1370 (2015)
2. Aylward, S.R., Jomier, J., Weeks, S., Bullitt, E.: Registration and analysis of vascular images. Int. J. Comput. Vis. **55**(2), 123–138 (2003)
3. Dibildox, G., Baka, N., Punt, M., Aben, J., Schultz, C., Niessen, W., van Walsum, T.: 3D/3D registration of coronary CTA and biplane XA reconstructions for improved image guidance. Med. Phys. **41**(9), 091909 (2014)
4. Von der Emde, G., Schwarz, S., Gomez, L., Budelli, R., Grant, K.: Electric fish measure distance in the dark. Nature **395**(6705), 890–894 (1998)
5. Gabriel, S., Lau, R., Gabriel, C.: The dielectric properties of biological tissues: II. Measurements in the frequency range 10 Hz to 20 GHz. Phys. Med. Biol. **41**(11), 2251–2269 (1996)
6. Groher, M., Zikic, D., Navab, N.: Deformable 2D–3D registration of vascular structures in a one view scenario. IEEE Trans. Med. Imaging **28**(6), 847–860 (2009)
7. Hettrick, D., Battocletti, J., Ackmann, J., Linehan, J., Waltier, D.: In vivo measurement of real-time aortic segmental volume using the conductance catheter. Ann. Biomed. Eng. **26**, 431–440 (1998)
8. Metzen, M., Biswas, S., Bousack, H., Gottwald, M., Mayekar, K., von der Emde, G.: A biomimetic active electrolocation sensor for detection of atherosclerotic lesions in blood vessels. IEEE Sens. J. **12**(2), 325–331 (2012)
9. Mitrovic, U., Spiclin, Z., Likar, B., Pernus, F.: 3D–2D registration of cerebral angiograms: a method and evaluation on clinical images. IEEE Trans. Med. Imaging **32**(8), 1550–1563 (2013)
10. Pauly, O., Heibel, H., Navab, N.: A machine learning approach for deformable guide-wire tracking in fluoroscopic sequences. In: Jiang, T., Navab, N., Pluim, J.P.W., Viergever, M.A. (eds.) MICCAI 2010, Part III. LNCS, vol. 6363, pp. 343–350. Springer, Heidelberg (2010)
11. Tormene, P., Giorgino, T., Quaglini, S., Stefanelli, M.: Matching incomplete time series with dynamic time warping: an algorithm and an application to post-stroke rehabilitation. Artif. Intell. Med. **45**, 11–34 (2009)
12. Choi, H.W., Zhang, Z., Farren, N., Kassab, G.: Implications of complex anatomical junctions on conductance catheter measurements of coronary arteries. J. Appl. Physiol. **114**(5), 656–664 (2013)